# Pharmacokinetic Analysis of $^{11}$C-PBR28 in the Rat Model of Herpes Encephalitis: Comparison with (*R*)-$^{11}$C-PK11195

Andrea Parente*[1], Paula Kopschina Feltes*[1,2], David Vállez García[1], Jurgen W.A. Sijbesma[1], Cristina M. Moriguchi Jeckel[2,3], Rudi A.J.O. Dierckx[1], Erik F.J. de Vries[1], and Janine Doorduin[1]

[1]*Department of Nuclear Medicine and Molecular Imaging, University of Groningen, University Medical Center Groningen, Groningen, The Netherlands;* [2]*Instituto de Geriatria e Gerontologia, Pontifícia Universidade Católica do Rio Grande do Sul, Porto Alegre, Brasil; and* [3]*Instituto do Cérebro do Rio Grande do Sul, Pontifícia Universidade Católica do Rio Grande do Sul, Porto Alegre, Brasil*

$^{11}$C-PBR28 is a second-generation translocator protein (TSPO) tracer with characteristics supposedly superior to the most commonly used tracer for neuroinflammation, (*R*)-$^{11}$C-PK11195. Despite its use in clinical research, no studies on the imaging properties and pharmacokinetic analysis of $^{11}$C-PBR28 in rodent models of neuroinflammation have been published yet. Therefore, this study aimed to evaluate $^{11}$C-PBR28 as a tool for detection and quantification of neuroinflammation in preclinical research and to compare its imaging properties with (*R*)-$^{11}$C-PK11195. The herpes simplex encephalitis (HSE) model was used for induction of neuroinflammation in male Wistar rats. Six or 7 d after virus inoculation, a dynamic $^{11}$C-PBR28 or (*R*)-$^{11}$C-PK11195 PET scan with arterial blood sampling was obtained. Pharmacokinetic modeling was performed on the PET data and analyzed using volumes of interest and a voxel-based approach. Volume-of-interest– and voxel-based analysis of $^{11}$C-PBR28 images showed overexpression of TSPO in brain regions known to be affected in the HSE rat model. $^{11}$C-PBR28 was metabolized faster than (*R*)-$^{11}$C-PK11195, with a metabolic half-life in plasma of 5 and 21 min, respectively. Overall, $^{11}$C-PBR28 was more sensitive than (*R*)-$^{11}$C-PK11195 in detecting neuroinflammation. The binding potential ($BP_{ND}$) of $^{11}$C-PBR28 was significantly higher ($P < 0.05$) in the medulla (176%), pons (146%), midbrain (101%), hippocampus (85%), thalamus (73%), cerebellum (54%), and hypothalamus (49%) in HSE rats than in control rats, whereas (*R*)-$^{11}$C-PK11195 showed a higher $BP_{ND}$ only in the medulla (32%). The $BP_{ND}$ in control animals was not significantly different between tracers, suggesting that the nonspecific binding of both tracers is similar. $^{11}$C-PBR28 was more sensitive than (*R*)-$^{11}$C-PK11195 in the detection of TSPO overexpression in the HSE rat model, because more brain regions with significantly increased tracer uptake could be found, irrespective of the data analysis method used. These results suggest that $^{11}$C-PBR28 should be able to detect more subtle changes in microglial activation in preclinical models of neuroinflammation.

**Key Words:** neuroinflammation; herpes simplex encephalitis; rat model; positron emission tomography; pharmacokinetic analysis

**J Nucl Med 2016; 57:785–791**
DOI: 10.2967/jnumed.115.165019

Microglia are the resident macrophages of the central nervous system (*1*). These immune cells are activated by inflammatory stimuli, such as pathogens or neuronal damage, and initiate a cascade of inflammatory responses. When microglia are activated, the expression of the 18-kDa translocator protein (TSPO) (*2*) on the outer mitochondrial membrane is increased. This increase in TSPO expression is also observed in infiltrating macrophages and activated astrocytes, cell types that both participate in the neuroinflammatory response. Under normal conditions TSPO expression in the brain is low. Therefore, TSPO overexpression can be used as a neuroinflammatory biomarker, which can be measured with noninvasive imaging techniques such as PET (*3*).

The oldest and most commonly used PET tracer for the detection of neuroinflammation is the TSPO ligand (*R*)-$^{11}$C-PK11195, which has been used in clinical and preclinical studies of various diseases and to evaluate new treatment strategies. However, this PET tracer has some limitations, including a low signal-to-noise ratio, poor bioavailability in brain tissue, high nonspecific binding, high variability in the pharmacokinetics and metabolism between subjects, high binding to plasma proteins, and low sensitivity to visualize mild inflammation (*4–6*).

To overcome some of the drawbacks associated with (*R*)-$^{11}$C-PK11195, second-generation TSPO PET tracers such as $^{11}$C-PBR28 have now been applied in clinical studies. $^{11}$C-PBR28 has better intrinsic characteristics for a PET tracer than (*R*)-$^{11}$C-PK11195, such as a higher affinity ($K_i$ = 0.2 vs. 0.8 nM) and lower lipophilicity (LogD = 3.01 ± 0.11 vs. 3.95 ± 0.18) (*7*). Consequently, $^{11}$C-PBR28 shows a higher TSPO-specific signal, which is beneficial for the follow-up of treatment strategies and the detection of mild neuroinflammation. Despite its superior imaging characteristics, $^{11}$C-PBR28 is still not the ideal TSPO tracer because of its sensitivity to the genotype of a single nucleotide polymorphism in the human TSPO gene (rs6971), with allele frequency of about 30% in Caucasians (*8*). Other second-generation high-affinity TSPO ligands, such as $^{18}$F-FEPPA (*9*), $^{18}$F-PBR06, $^{18}$F-PBR111, $^{18}$F-DPA-714, $^{11}$C-DPA-113, and $^{11}$C-DAA1106 (*10–12*), are also to some extent sensitive to this polymorphism, which is a major limitation for their use in clinical studies.

To our knowledge, there are no studies that have demonstrated the presence of TSPO polymorphism in rodents. Therefore, $^{11}$C-PBR28 could be an attractive PET tracer for preclinical imaging studies in animal models of neuroinflammation. However, only 2 studies have evaluated $^{11}$C-PBR28 for PET imaging of neuroinflammation in rodent models (*13,14*). None of those studies compared the $^{11}$C-PBR28 imaging results with those of (*R*)-$^{11}$C-PK11195.

The aim of the present study was to evaluate $^{11}$C-PBR28 as a TSPO PET tracer for preclinical imaging in the herpes simplex

Received Aug. 3, 2015; revision accepted Dec. 4, 2015.
For correspondence or reprints contact: Janine Doorduin, University of Groningen, University Medical Center Groningen, Hanzeplein 1, Groningen, 9700 RB, The Netherlands.
E-mail: j.doorduin@umcg.nl
*Contributed equally to this work.
Published online Jan. 28, 2016.

encephalitis (HSE) model (*15*). In this rat model, neuroinflammation is caused by intranasal inoculation of the herpes simplex virus type 1 (HSV-1) (*15,16*) and does not require a surgical procedure that could damage the integrity of the blood–brain barrier. The in vivo pharmacokinetics and metabolism of $^{11}$C-PBR28 were investigated and compared with (*R*)-$^{11}$C-PK11195.

## MATERIALS AND METHODS

### Rats

Male outbred Wistar-Unilever rats (age, 6–8 wk; weight, 299 ± 25 g) were obtained from Harlan. The rats were allowed to acclimatize for at least 7 d before the start of the experiment. Rats were housed individually in Makrolon cages, containing a layer of wood shavings. The room was kept on constant temperature (21 ± 2°C) with a 12–12 h light–dark regimen. Water and commercial chow were available ad libitum.

All animal experiments were performed according to the Dutch Law for Animal Welfare and were approved by the Institutional Animal Care and Use Committee of the University of Groningen (DEC 6264A and 6264C).

### Animal Model

An HSV-1 strain was obtained from a clinical isolate, cultured in Vero cells, and assayed for plaque-forming units per milliliter. Rats were slightly anesthetized with 5% isoflurane mixed with medical air, and 50 μL of phosphate-buffered saline containing $1 \times 10^7$ plaque-forming units of HSV-1 were pipetted into each nostril (*15*). The same procedure was applied to control rats using phosphate-buffered saline without the virus. Clinical symptoms were scored daily by the same observer.

### Study Design

Rats were randomly divided in the control group ($n = 6$) and HSE group ($n = 6$). $^{11}$C-PBR28 PET scans with arterial blood sampling were obtained on day 6 or 7 after inoculation. The (*R*)-$^{11}$C-PK11195 PET data were acquired in a previous study using identical methods (*16*) but completely reanalyzed for this study.

### Tracer Synthesis

$^{11}$C-PBR28 was synthesized following a previously described procedure (*17*), with slight modifications. The precursor was dissolved in 300 μL of dimethyl-sulfoxide instead of acetonitrile, and 10 mg of potassium hydroxide were used as base instead of sodium hydride. The use of potassium hydroxide required the addition of 200 μL of 0.1 M hydrochloric acid after the reaction for neutralization. A filtration step was added before high-performance liquid chromatography purification. The final product (pH 6.5–7) was obtained in 39% ± 6% radiochemical yield (corrected for decay), with a radiochemical purity of 100% and a specific activity of 196 ± 35 GBq/μmol.

### PET Imaging with Arterial Blood Sampling

Rats were anesthetized with isoflurane in medical air (5% for induction, 2%–3% for maintenance). A cannula was placed in the femoral artery for blood sampling, and another was inserted in the femoral vein for tracer injection. The rats were placed into the PET camera (Focus 220; Siemens Medical Solutions Inc.) with their head in the field of view. Body temperature was maintained with heating pads, and heart rate and oxygen saturation were monitored during the scan. A transmission scan was acquired using a $^{57}$Co point source for attenuation and scatter correction. $^{11}$C-PBR28 (68 ± 21 MBq; 0.67 ± 0.11 nmol) was injected over 1 min, using an automatic pump at a speed of 1 mL/min, and a 91-min dynamic PET scan was acquired.

During the first 60 min of the scan, 16 blood samples of 0.1 mL were taken at 10, 20, 30, 40, 50, 60, 90, 120, 180, 300, 450, 600, 900, 1,800, 2,700, and 3,600 s after tracer injection. After collection of the blood samples, the same volume of heparinized saline was injected to prevent large changes in blood pressure. A 25-μL aliquot of whole blood was taken from each sample for radioactivity measurement (whole-blood curve). The remainder of the sample was centrifuged at 13,000 rpm (16,000*g*) for 8 min, and 25 μL of plasma were taken for radioactivity measurement. The radioactivity in blood and plasma was measured with a γ-counter (LKB-Wallac) and corrected for decay.

### Tracer Displacement

Displacement of $^{11}$C-PBR28 was evaluated by administration of an excess of PK11195 during the PET scan. Thus, unlabeled PK11195 (5 mg/kg) in 200 μL of dimethyl-sulfoxide was intravenously injected over a period of 1 min via the venous cannula at 61 min after tracer injection. PET acquisition was continued for another 30 min without blood sampling.

### Metabolite Analysis

The percentage of intact tracer in plasma was measured for blood samples (0.6 mL) collected at 3, 5, 7.5, 10, 15, 30, 45, or 60 min after tracer injection. Two or 3 samples were collected from each animal. Immediately after collection, the blood samples were placed on ice to inhibit tracer metabolism (*18*). Centrifugation and collection of the plasma sample were performed as described above. Plasma was diluted and mixed with an equal volume of acetonitrile. The samples were centrifuged for 3 min at 5,300 rpm (3,000*g*). The supernatant was filtered through a Millipore Millex-HV filter (4 mm; pore size, 0.45 μm) and analyzed by high-performance liquid chromatography using an Alltima RP-C18 column (5 μm, 10 × 250 mm) and a mobile phase consisting of acetonitrile/water (50/50) at a flow of 5 mL/min. Fractions of 30 s were collected and measured in the γ-counter.

The metabolite data of all animals were grouped to generate a single population curve, because no statistical difference in tracer metabolism and in parent fraction of each tracer between the groups was found. The data points of the percentage of intact tracer versus time were fitted with a 1-phase exponential function. The individual plasma radioactivity values were corrected for the percentage of intact tracer and used together with the whole blood for pharmacokinetic analysis.

### PET Image Reconstruction and Preparation

The list-mode data from the first 60 min of the emission scan were reconstructed into 21 frames (6 × 10, 4 × 30, 2 × 60, 1 × 120, 1 × 180, 4 × 300, and 3 × 600 s). For the displacement study, the last 31 min of the PET scan were reconstructed into 19 frames (1 × 60, 6 × 10, 4 × 30, 2 × 60, 1 × 120, 1 × 180, and 4 × 300 s). Emission sinograms were iteratively reconstructed (2-dimensional ordered-subset expectation maximization, 4 iterations and 16 subsets) after being normalized and corrected for attenuation and decay of radioactivity.

PET images were analyzed using PMOD 3.5 software (PMOD Technologies Ltd.). The scans were automatically registered to tracer-specific PET templates (*19*). Volumes of interest (VOIs) of several brain regions were constructed on the basis of previously defined structures (*19*). The brain radioactivity concentration was calculated from the VOIs to generate time–activity curves and expressed as SUVs: (tissue activity concentration [MBq/g] × body weight [g])/(injected dose [MBq]). The 50- to 60-min time frame was used for VOI- and voxel-based statistical analysis (*20*).

### Pharmacokinetic Analysis

Pharmacokinetic modeling analysis was performed in PMOD, using the whole-blood and metabolite-corrected plasma curves as input functions. Visual inspection showed a better fit for Logan graphical analysis, confirming the reversible behavior of the tracer (*21*), using a t* of 15 min, and the Logan analysis was used to calculate the distribution volume ($V_T$). In addition, the reversible 2-tissue-compartment model (2TCM) was calculated with the equation

$$\frac{dC_1(t)}{dt} = K_1 C_p(t) - (k_2 + k_3) C_1(t) + k_4 C_2(t)$$
$$\frac{dC_2(t)}{dt} = k_3 C_1(t) - k_4 C_2(t),$$

where $C_p$, $C_1$, and $C_2$ represent the tracer concentration in plasma and tissue compartments 1 and 2, respectively. A fixed blood volume of

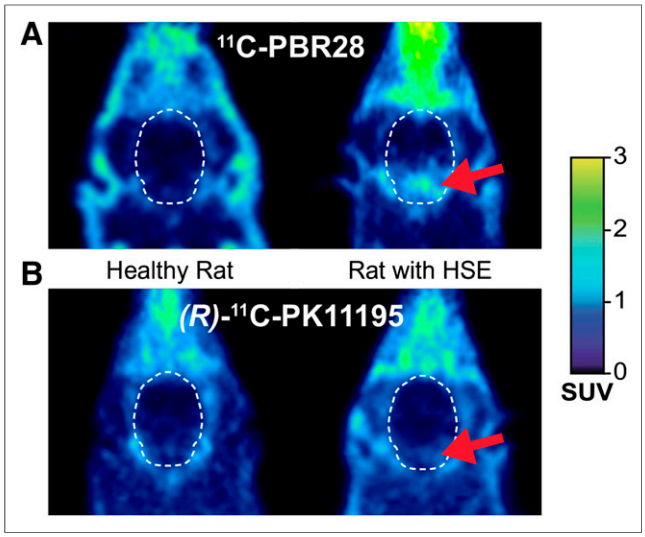


**FIGURE 1.** Transaxial $^{11}$C-PBR28 (A) and (*R*)-$^{11}$C-PK11195 (B) PET images (30–60 min) of head of control rat and HSE rat. Arrow shows increased uptake in region of pons and medulla.

3.6% (*22*) was used for the calculation, and $V_T$ and nondisplaceable binding potential ($BP_{ND}$ calculated as $k_3/k_4$) were obtained (*23*).

### Statistical Analysis

Results are presented as mean ± SD. Statistical analysis was performed using IBM SPSS Statistics 20. Differences between groups were analyzed by independent-sample *t* tests and considered to be significant with a *P* value of less than 0.05, without correction for multiple comparisons.

Voxel-based analysis was performed using SPM12 (Wellcome Trust Centre for Neuroimaging) and SAMIT toolbox (*19*). Images were smoothed with a 1.2-mm isotropic gaussian kernel. Statistical analysis was performed using a 2-sample *t* test design (control vs. HSE) without global normalization. For evaluation of group differences, T-map data were interrogated at a *P* value of less than 0.005 (uncorrected) and an extent threshold of 200 voxels. Only those clusters with a *P* value of less than 0.05 corrected for familywise error were considered significant.

The magnitude of difference between groups was assessed using the Cohen's *d* effect size index, calculated for VOI analysis as $d = (\text{mean HSE} - \text{mean control})/\sqrt{(\text{SD HSE}^2 + \text{SD control}^2)/2}$ and for voxel-based analysis as $d = (2T - \text{value})/\sqrt{df}$.

## RESULTS

### VOI-Based Analysis

The uptake of $^{11}$C-PBR28 in several brain regions of HSE rats corresponded with the distribution pattern of the viral infection (Fig. 1) (*15*). VOI-based analysis showed significantly higher whole-brain $^{11}$C-PBR28 uptake in HSE rats than in control rats (+44%, $P = 0.032$, Table 1). Analysis of individual brain regions revealed an increased uptake of $^{11}$C-PBR28 in the pons (+150%, $P = 0.016$), medulla (+144%, $P = 0.015$), and hypothalamus (+44%, $P = 0.034$).

### Voxel-Based Analysis

Voxel-based analysis showed a large cluster with a significantly higher $^{11}$C-PBR28 uptake in the HSE group than in the control group (Fig. 2; Table 2). This cluster included bilaterally the pons, medulla, midbrain, hippocampus, cerebellum, and hypothalamus.

**TABLE 1**
$^{11}$C-PBR28 Uptake (50–60 Minutes), Expressed as SUV (Mean ± SD), Obtained by PET Imaging of Control and HSE Groups

| Brain region | Control | HSE | *d* |
|---|---|---|---|
| Amygdala | 0.45 ± 0.08 | 0.56 ± 0.10 | |
| Cerebellum | 0.64 ± 0.11 | 0.98 ± 0.37 | |
| Frontal cortex | 0.53 ± 0.05 | 0.73 ± 0.24 | |
| Hippocampus | 0.42 ± 0.06 | 0.56 ± 0.14 | |
| Hypothalamus | 0.42 ± 0.10 | 0.61 ± 0.14* | 1.56 |
| Medulla | 0.64 ± 0.11 | 1.56 ± 0.52* | 2.45 |
| Midbrain | 0.44 ± 0.06 | 0.76 ± 0.30 | |
| Pons | 0.50 ± 0.11 | 1.25 ± 0.44* | 2.34 |
| Septum | 0.47 ± 0.05 | 0.53 ± 0.08 | |
| Striatum | 0.38 ± 0.06 | 0.43 ± 0.08 | |
| Thalamus | 0.41 ± 0.04 | 0.54 ± 0.13 | |
| Whole brain | 0.52 ± 0.07 | 0.75 ± 0.17* | 1.77 |

*$P < 0.05$.
*d* = Cohen's effect size.

### Displacement

The time–activity curves of the medulla and frontal cortex are shown in Figure 3, representing an infected and a noninfected brain region, respectively. Injection of 5 mg/kg of PK11195 at 60 min caused an initial increase in tracer uptake in all brain regions due to the release of $^{11}$C-PBR28 from peripheral organs with TSPO expression, such as lungs, heart, glands, and blood vessels (*15*). $^{11}$C-PBR28 uptake in the medulla of HSE rats was significantly lower 10 min after PK11195 injection than just before displacement (51% and 68% at 10 and 30 min after displacement, respectively, $P < 0.05$). No significant reduction in $^{11}$C-PBR28 uptake in the medulla of control rats was observed. Moreover, injection of PK11195 did not significantly reduce $^{11}$C-PBR28 uptake in the frontal cortex of HSE or control rats.

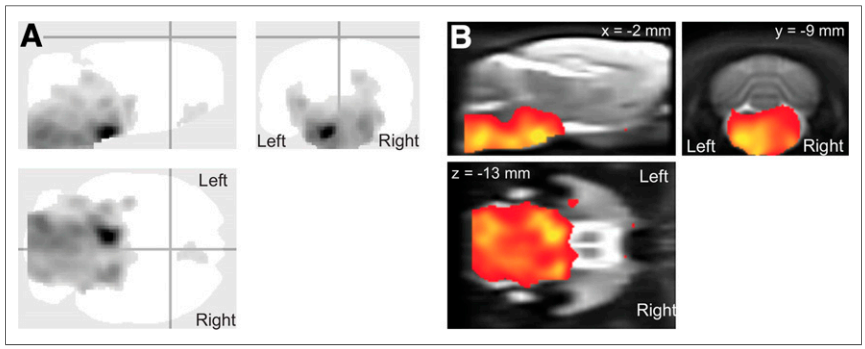


**FIGURE 2.** $^{11}$C-PBR28 voxel-based analysis results displayed as glass brain (A), showing areas with significantly higher uptake in HSE group than in control group (B) ($P < 0.05$ familywise error corrected at cluster level).

**TABLE 2**
Brain Regions Showing Increased $^{11}$C-PBR28 Uptake in Voxel-Based Analysis

| Brain region | No. of voxels | T value (mean ± SD) | *d* |
|---|---|---|---|
| Medulla | 6,886 | 4.58 ± 0.81 | 3.05 |
| Pons | 5,241 | 4.46 ± 0.80 | 2.97 |
| Midbrain | 2,485 | 3.76 ± 0.42 | 2.51 |
| Hippocampus | 1,041 | 3.83 ± 0.49 | 2.55 |
| Cerebellum | 886 | 3.55 ± 0.26 | 2.37 |
| Hypothalamus | 623 | 3.65 ± 0.33 | 2.43 |

*d* = Cohen's effect size.

### Tracer Metabolism

Metabolite analysis revealed that $^{11}$C-PBR28 was metabolized faster than (*R*)-$^{11}$C-PK11195 (Fig. 4), with 50% of plasma radioactivity consisting of metabolites at 5 and 21 min after injection of $^{11}$C-PBR28 and (*R*)-$^{11}$C-PK11195, respectively. The whole-blood and metabolite-corrected plasma curves showed that $^{11}$C-PBR28 presented higher whole blood, but substantially lower plasma activity, after correction for metabolites than (*R*)-$^{11}$C-PK11195.

### Kinetic Modeling

For both $^{11}$C-PBR28 and (*R*)-$^{11}$C-PK11195, the $V_T$ obtained from the 2TCM showed an excellent correlation ($r^2$ = 0.95 and 0.98, respectively; $P < 0.001$), with the $V_T$ obtained from Logan graphical analysis (Fig. 5). $V_T$ values of $^{11}$C-PBR28 were approximately 5-fold higher than those of (*R*)-$^{11}$C-PK11195, irrespective of the group or brain area.

Because $^{11}$C-PBR28 and (*R*)-$^{11}$C-PK11195 are receptor tracers, $BP_{ND}$ was chosen as the main outcome parameter. No statistical differences were found between the $BP_{ND}$ of $^{11}$C-PBR28 and (*R*)-$^{11}$C-PK11195 in any brain regions of control rats. For both tracers, whole-brain $BP_{ND}$ was significantly higher in HSE rats than in controls (Table 3). The $BP_{ND}$ of $^{11}$C-PBR28 was significantly higher in several brain regions of HSE rats than in control rats, in particular in the medulla (+176%, $P < 0.001$), pons (+146%, $P < 0.001$), midbrain (+101, $P = 0.001$), hippocampus (85%, $P < 0.05$), thalamus (+73%, $P < 0.05$), cerebellum (+54%, $P < 0.05$), and hypothalamus (+49%, $P < 0.05$). In contrast, (*R*)-$^{11}$C-PK11195 showed a significantly higher $BP_{ND}$ only in the medulla (+32%, $P < 0.01$) of HSE rats as compared with controls.

### Correlation Between Tracer Uptake Parameters

To assess whether a simplified procedure without blood sampling could be applied to quantify tracer uptake, the SUVs of $^{11}$C-PBR28 and (*R*)-$^{11}$C-PK11195 in different brain regions were correlated with the $V_T$ and $BP_{ND}$ obtained from Logan and 2TCM kinetic analysis, respectively (Fig. 6). The SUVs of $^{11}$C-PBR28 showed a moderate correlation ($r^2$ = 0.463, $P < 0.001$) with $BP_{ND}$ values. In contrast, a strong correlation was found between the SUV and $V_T$ of $^{11}$C-PBR28 ($r^2$ = 0.87, $P < 0.001$). For (*R*)-$^{11}$C-PK11195, only modest correlations were found between the SUV and the $BP_{ND}$ ($r^2$ = 0.133, $P < 0.001$) and between the SUV and the $V_T$ ($r^2$ = 0.143, $P < 0.001$).

## DISCUSSION

$^{11}$C-PBR28 is a second-generation PET tracer for TSPO imaging that has already been applied in clinical studies but surprisingly has not been fully evaluated in a rodent model of neuroinflammation yet. In this study, the performance of $^{11}$C-PBR28 for the preclinical imaging of neuroinflammation was evaluated with the HSE model, with (*R*)-$^{11}$C-PK11195 tracer used for comparison purposes. In the HSE model, nasal infection with HSV-1 induces strong activation of microglia 6–7 d after infection, in particular in the pons and medulla (*15,16,24*). $^{11}$C-PBR28 was able to detect the activation of microglia in more brain regions and proved to be more sensitive than (*R*)-$^{11}$C-PK11195. This difference between tracers might be due to the higher affinity of $^{11}$C-PBR28 for TSPO than (*R*)-$^{11}$C-PK11195. VOI-based analysis of predefined brain regions demonstrated an increased $^{11}$C-PBR28 uptake in the medulla, pons, and hippocampus in HSE rats when compared with controls. The enhanced $^{11}$C-PBR28 uptake in these brain regions could be displaced by administration of PK11195 (5 mg/kg), resulting in tracer concentrations that were comparable to controls. This demonstrates that the increased uptake of $^{11}$C-PBR28 in the infected brain areas represents increased specific binding to TSPO and is not solely due to other inflammatory phenomena, such as increased cerebral blood flow (*13*).

Voxel-based analysis, compared with VOI-based, has the capacity to identify affected brain region not limited to predefined regions. In this study, voxel-based analysis showed more brain regions with increased $^{11}$C-PBR28 uptake than VOI-based analysis. Besides the medulla, pons, and hypothalamus, significantly increased $^{11}$C-PBR28 uptake was found in the midbrain,

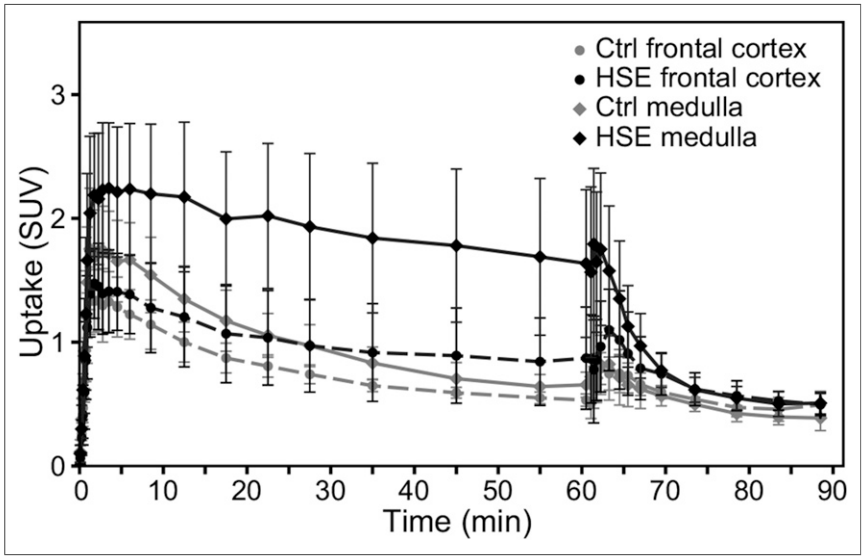


**FIGURE 3.** $^{11}$C-PBR28 time–activity curves of medulla and frontal cortex from HSE and control groups. Rats were injected with PK11195 60 (5 mg/kg) min after tracer injection to displace bound tracer from TSPO. Ctrl = control.

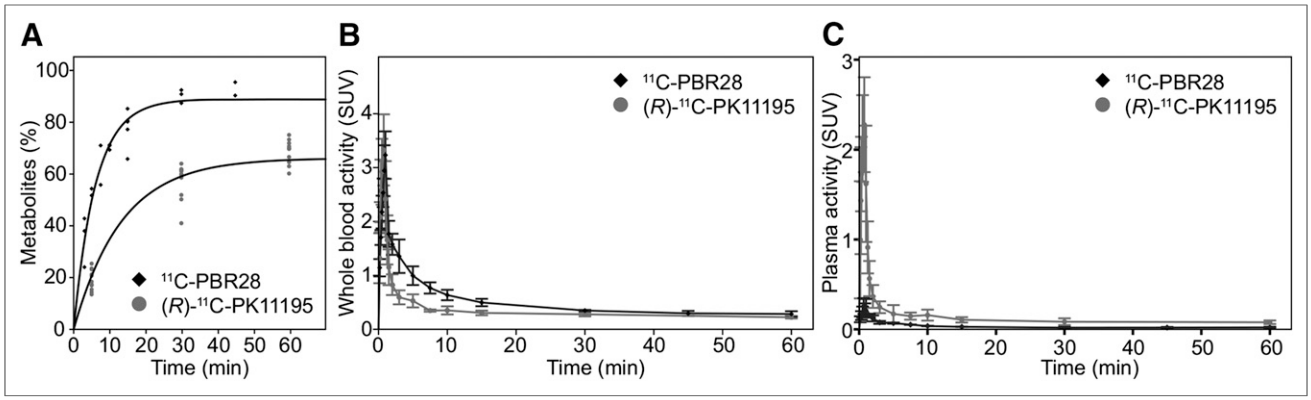


**FIGURE 4.** Percentage of metabolites present in plasma (A) and whole blood (B), and metabolite-corrected plasma curves (C) of $^{11}$C-PBR28 and (*R*)-$^{11}$C-PK11195.

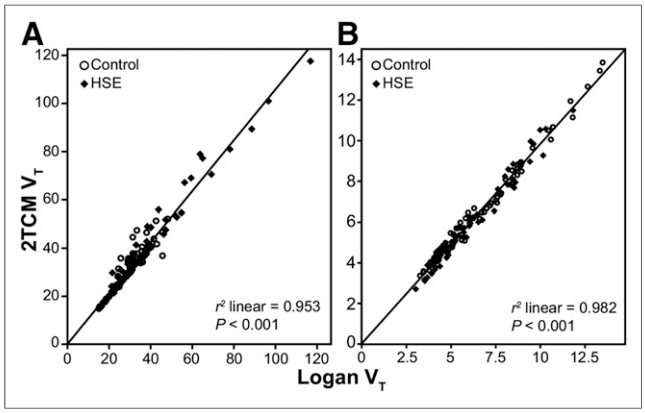


**FIGURE 5.** Correlation of $V_T$ of individual brain regions determined by 2TCM and Logan graphical analysis for $^{11}$C-PBR28 (A) and (*R*)-$^{11}$C-PK11195 (B).

hippocampus, and cerebellum. These results indicate that voxel-based analysis is a more sensitive method to detect focal neuroinflammation.

For the pharmacokinetic modeling, blood sampling and metabolite analysis were performed for both tracers. $^{11}$C-PBR28 proved to be metabolized substantially faster than (*R*)-$^{11}$C-PK11195. However, only polar metabolites of $^{11}$C-PBR28 were formed and these radioactive metabolites practically do not enter the brain, as demonstrated by Briard et al. (*7*). At 30 min after injection, 97.6% of the radioactivity in the brain consisted of intact tracer, with the small percentage of metabolites in the brain likely originating from the blood compartment. Interestingly, the activity of $^{11}$C-PBR28 in plasma is much lower than in whole blood. This might be explained by the presence of TSPO receptors in red blood cells, which can bind the tracer. This binding seems to be more important for the second-generation TSPO

**TABLE 3**
$^{11}$C-PBR28 and (*R*)-$^{11}$C-PK11195 Binding Potential (Mean ± SD) of Control and HSE Rats

| | $^{11}$C-PBR28 | | | (*R*)-$^{11}$C-PK11195 | | |
|---|---|---|---|---|---|---|
| Brain region | Control | HSE | *d* | Control | HSE | *d* |
| Amygdala | 1.24 ± 0.12 | 2.03 ± 0.48* | 2.3 | 1.67 ± 0.35 | 1.84 ± 0.54 | |
| Cerebellum | 1.94 ± 0.34 | 3.00 ± 0.70* | 1.9 | 2.10 ± 0.53 | 2.09 ± 0.57 | |
| Cortex frontal | 1.55 ± 0.45 | 2.61 ± 0.93 | | 1.90 ± 0.61 | 2.01 ± 0.59 | |
| Hippocampus | 1.08 ± 0.26 | 2.00 ± 0.63† | 1.9 | 1.42 ± 0.30 | 1.83 ± 0.63 | |
| Hypothalamus | 1.12 ± 0.27 | 1.69 ± 0.34* | 1.9 | 1.63 ± 0.35 | 1.42 ± 0.50 | |
| Medulla | 1.43 ± 0.26 | 3.95 ± 0.55‡ | 5.9 | 1.74 ± 0.30 | 2.30 ± 0.25† | 2.0 |
| Midbrain | 1.12 ± 0.27 | 2.26 ± 0.52‡ | 2.8 | 1.62 ± 0.60 | 2.20 ± 0.81 | |
| Pons | 1.30 ± 0.42 | 3.19 ± 0.42‡ | 5.0 | 1.88 ± 0.45 | 2.05 ± 0.66 | |
| Septum | 1.19 ± 0.42 | 1.87 ± 0.55 | | 1.67 ± 0.35 | 1.49 ± 0.57 | |
| Striatum | 1.04 ± 0.24 | 1.87 ± 0.55 | | 1.22 ± 0.29 | 1.30 ± 0.53 | |
| Thalamus | 1.05 ± 0.24 | 1.81 ± 0.60* | 1.7 | 1.29 ± 0.30 | 1.68 ± 0.43 | |
| Whole brain | 1.53 ± 0.36 | 2.63 ± 0.47† | 2.6 | 1.48 ± 0.33 | 1.73 ± 0.60 | |

*$P < 0.05$.
†$P < 0.01$.
‡$P < 0.001$.
*d* = Cohen's effect size.

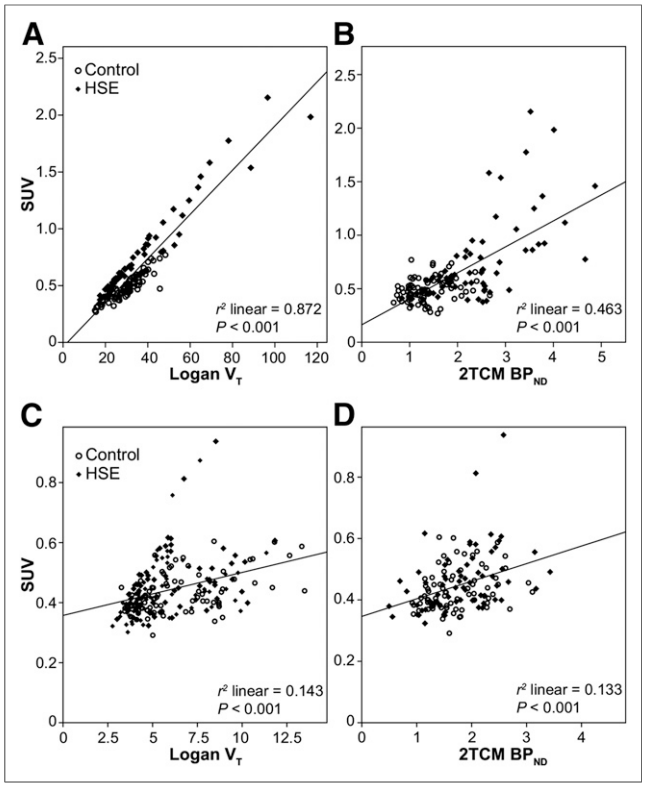


**FIGURE 6.** Correlations between SUV and $V_T$ values (A) and SUV and $BP_{ND}$ values (B) of $^{11}$C-PBR28, and between SUV and $V_T$ values (C) and SUV and $BP_{ND}$ values (D) of (*R*)-$^{11}$C-PK11195 in HSE and control rats.

tracers with higher affinity for TSPO (e.g., $^{11}$C-PBR28) than for (*R*)-$^{11}$C-PK11195 (*25*).

The 2TCM is considered the most suitable model for pharmacokinetic analysis of the receptor ligands $^{11}$C-PBR28 (*26*) and (*R*)-$^{11}$C-PK11195 (*27*). $BP_{ND}$ was used as the main outcome because it represents the specific binding of the tracer to the TSPO receptor. $^{11}$C-PBR28 was able to detect a statistically significant increase in $BP_{ND}$ in affected brain regions, such as the medulla, pons, cerebellum, midbrain, thalamus, hippocampus, and hypothalamus. In contrast, the $BP_{ND}$ of (*R*)-$^{11}$C-PK11195 was significantly increased only in the medulla of HSE rats. Comparison of the $BP_{ND}$ of both tracers in control animals showed no significant difference, suggesting that binding of both tracers under normal physiologic conditions is similar (*16*). $V_T$ values of $^{11}$C-PBR28 calculated by Logan analysis and 2TCM were highly correlated but seem less suitable as outcome parameters because of their high intersubject variability (Supplemental Table 1; Supplemental Fig. 1 [supplemental materials are available at http://jnm.snmjournals.org]) (*14,28*), which may be attributed to variations in the $K_1/k_2$ (perfusion may be altered in neuroinflammatory processes) or to variations in plasma availability of $^{11}$C-PBR28 (*20*). Consequently, $V_T$ comparison between groups was not performed in the current study. A possible limitation of the current study is the lack of measurement of the plasma free fraction (fP). However, previously high variability in fP was found (25%–35%) (*29*), increasing the intersubject variability in $V_T$. Consequently, the added error by including fP was greater than the correction it represented.

To simplify the imaging procedure while retaining reliable quantitative information, the $V_T$ and $BP_{ND}$ values were correlated with SUVs, which can easily be obtained without blood sampling. SUVs of $^{11}$C-PBR28 showed a moderate correlation with $BP_{ND}$ but are strongly correlated with $V_T$. This can be explained by the fact that SUV and $V_T$ can both be influenced by different factors (e.g., the delivery of the tracer or the cerebral blood flow), whereas $BP_{ND}$ is only dependent on specific receptor binding and its release. Therefore, SUVs might better reflect the total $V_T$ than the binding potential for $^{11}$C-PBR28. For (*R*)-$^{11}$C-PK11195, the SUV showed a poor correlation with both $BP_{ND}$ and $V_T$.

## CONCLUSION

The present study demonstrated that $^{11}$C-PBR28 was able to detect TSPO overexpression in the encephalitic rat brain model. The most sensitive analysis methods to detect infected brain areas were either voxel-based analysis of static scans or the assessment of $BP_{ND}$ by full pharmacokinetic analysis of dynamic PET data. $^{11}$C-PBR28 has a better sensitivity toward areas with overexpression of TSPO than (*R*)-$^{11}$C-PK11195. $^{11}$C-PBR28 not only detected more brain regions with neuroinflammation, but also showed a larger increase in $BP_{ND}$ in infected areas than (*R*)-$^{11}$C-PK11195. A higher sensitivity for detection of TSPO overexpression implies that milder neuroinflammation and smaller changes might be better detected; therefore, disease processes and novel treatment strategies could be better monitored in preclinical models.

## DISCLOSURE

The costs of publication of this article were defrayed in part by the payment of page charges. Therefore, and solely to indicate this fact, this article is hereby marked "advertisement" in accordance with 18 USC section 1734. Financial support for this work was provided by Siemens Medical Solutions Inc. No other potential conflict of interest relevant to this article was reported.

## ACKNOWLEDGMENTS

We thank Bram Maas, Rolf Zijlma, Luís Juarez Orozco, and Inês Farinha Antunes for their support.

## REFERENCES

1. Frick LR, Williams K, Pittenger C. Microglial dysregulation in psychiatric disease. *Clin Dev Immunol.* 2013;2013:1–10.
2. Papadopoulos V, Baraldi M, Guilarte TR, et al. Translocator protein (18kDa): new nomenclature for the peripheral-type benzodiazepine receptor based on its structure and molecular function. *Trends Pharmacol Sci.* 2006;27:402–409.
3. Venneti S, Lopresti BJ. Wiley C a. The peripheral benzodiazepine receptor (translocator protein 18kDa) in microglia: from pathology to imaging. *Prog Neurobiol.* 2006;80:308–322.
4. Schweitzer PJ, Fallon BA, Mann JJ, Kumar JSD. PET tracers for the peripheral benzodiazepine receptor and uses thereof. *Drug Discov Today.* 2010;15:933–942.
5. Trapani A, Palazzo C, De Candia M, Lasorsa FM, Trapani G. Targeting of the translocator protein 18 kDa (TSPO): a valuable approach for nuclear and optical imaging of activated microglia. *Bioconjug Chem.* 2013;24:1415–1428.
6. Chauveau F, Boutin H, Van Camp N, Dollé F, Tavitian B. Nuclear imaging of neuroinflammation: a comprehensive review of [$^{11}$C]PK11195 challengers. *Eur J Nucl Med Mol Imaging.* 2008;35:2304–2319.

7. Briard E, Zoghbi SS, Imaizumi M, et al. Synthesis and evaluation in monkey of two sensitive $^{11}$C-labeled aryloxyanilide ligands for imaging brain peripheral benzodiazepine receptors in vivo. *J Med Chem.* 2008;51:17–30.
8. Kreisl WC, Jenko KJ, Hines CS, et al. A genetic polymorphism for translocator protein 18 kDa affects both in vitro and in vivo radioligand binding in human brain to this putative biomarker of neuroinflammation. *J Cereb Blood Flow Metab.* 2013;33:53–58.
9. Setiawan E, Wilson AA, Mizrahi R, et al. Role of translocator protein density, a marker of neuroinflammation, in the brain during major depressive episodes. *JAMA Psychiatry.* 2015;72:268–275.
10. Owen DRJ, Gunn RN, Rabiner EA, et al. Mixed-affinity binding in humans with 18-kDa translocator protein ligands. *J Nucl Med.* 2011;52:24–32.
11. Owen DR, Yeo AJ, Gunn RN, et al. An 18-kDa translocator protein (TSPO) polymorphism explains differences in binding affinity of the PET radioligand PBR28. *J Cereb Blood Flow Metab.* 2012;32:1–5.
12. Owen DR, Howell OW, Tang S-P, et al. Two binding sites for [$^{3}$H]PBR28 in human brain: implications for TSPO PET imaging of neuroinflammation. *J Cereb Blood Flow Metab.* 2010;30:1608–1618.
13. Imaizumi M, Kim HJ, Zoghbi SS, et al. PET imaging with [$^{11}$C]PBR28 can localize and quantify upregulated peripheral benzodiazepine receptors associated with cerebral ischemia in rat. *Neurosci Lett.* 2007;411:200–205.
14. Walker MD, Dinelle K, Kornelsen R, et al. [$^{11}$C]PBR28 PET imaging is sensitive to neuroinflammation in the aged rat. *J Cereb Blood Flow Metab.* 2015;35:1331–1338.
15. Doorduin J, Klein HC, Dierckx RA, James M, Kassiou M, de Vries EFJ. [$^{11}$C]-DPA-713 and [$^{18}$F]-DPA-714 as new PET tracers for TSPO: a comparison with [$^{11}$C]-(R)-PK11195 in a rat model of herpes encephalitis. *Mol Imaging Biol.* 2009;11:386–398.
16. Vállez Garcia D, de Vries EFJ, Toyohara J, et al. Evaluation of [$^{11}$C]CB184 for imaging and quantification of TSPO overexpression in a rat model of herpes encephalitis. *Eur J Nucl Med Mol Imaging.* 2015;42:1106–1118.
17. Wang M, Yoder KK, Gao M, et al. Fully automated synthesis and initial PET evaluation of [$^{11}$C]PBR28. *Bioorg Med Chem Lett.* 2009;19:5636–5639.
18. Yin P, Peter A, Franken H, et al. Preanalytical aspects and sample quality assessment in metabolomics studies of human blood. *Clin Chem.* 2013;59:833–845.
19. Vállez Garcia D, Casteels C, Schwarz AJ, Dierckx RAJO, Koole M, Doorduin J. A standardized method for the construction of tracer specific PET and SPECT rat brain templates: validation and implementation of a toolbox. *PLoS One.* 2015;10:e0122363.
20. Tóth M, Doorduin J, Häggkvist J, et al. Positron emission tomography studies with [$^{11}$C]PBR28 in the healthy rodent brain: validating SUV as an outcome measure of neuroinflammation. *PLoS One.* 2015;10:e0125917.
21. Logan J, Fowler JS, Volkow ND, et al. Graphical analysis of reversible radioligand binding from time-activity measurements applied to [N-$^{11}$C-methyl]-(-)-cocaine PET studies in human subjects. *J Cereb Blood Flow Metab.* 1990;10:740–747.
22. Julien-Dolbec C, Tropres I, Montigon O, et al. Regional response of cerebral blood volume to graded hypoxic hypoxia in rat brain. *Br J Anaesth.* 2002;89:287–293.
23. Innis RB, Cunningham VJ, Delforge J, et al. Consensus nomenclature for in vivo imaging of reversibly binding radioligands. *J Cereb Blood Flow Metab.* 2007;27:1533–1539.
24. Esiri MM, Drummond CWE, Morris CS. Macrophages and microglia in HSV-1 infected mouse brain. *J Neuroimmunol.* 1995;62:201–205.
25. Rizzo G, Veronese M, Tonietto M, Zanotti-Fregonara P, Turkheimer FE, Bertoldo A. Kinetic modeling without accounting for the vascular component impairs the quantification of [$^{11}$C]PBR28 brain PET data. *J Cereb Blood Flow Metab.* 2014;34:1060–1069.
26. Owen DR, Guo Q, Kalk NJ, et al. Determination of [$^{11}$C]PBR28 binding potential in vivo: a first human TSPO blocking study. *J Cereb Blood Flow Metab.* 2014;34:989–994.
27. Kropholler MA, Boellaard R, Schuitemaker A, et al. Development of a tracer kinetic plasma input model for (R)-[$^{11}$C]PK11195 brain studies. *J Cereb Blood Flow Metab.* 2005;25:842–851.
28. Suridjan I, Rusjan PM, Voineskos AN, et al. Neuroinflammation in healthy aging: a PET study using a novel translocator protein 18kDa (TSPO) radioligand, [$^{18}$F]-FEPPA. *Neuroimage.* 2014;84:868–875.
29. Bloomfield PS, Selvaraj S, Veronese M, et al. Microglial activity in people at ultra high risk of psychosis and in schizophrenia: an [$^{11}$ C]PBR28 PET brain imaging study. *Am J Psychiatry.* 2015;173:44–52.

The Journal of NUCLEAR MEDICINE

# Pharmacokinetic Analysis of $^{11}$C-PBR28 in the Rat Model of Herpes Encephalitis: Comparison with (*R*)-$^{11}$C-PK11195

Andrea Parente, Paula Kopschina Feltes, David Vállez García, Jurgen W.A. Sijbesma, Cristina M. Moriguchi Jeckel, Rudi A.J.O. Dierckx, Erik F.J. de Vries and Janine Doorduin

*J Nucl Med.* 2016;57:785-791.
Published online: January 28, 2016.
Doi: 10.2967/jnumed.115.165019



*The Journal of Nuclear Medicine* is published monthly.
SNMMI | Society of Nuclear Medicine and Molecular Imaging
1850 Samuel Morse Drive, Reston, VA 20190.
(Print ISSN: 0161-5505, Online ISSN: 2159-662X)



SNMMI SOCIETY OF NUCLEAR MEDICINE AND MOLECULAR IMAGING